

# Enhancing Singlet Fission Dynamics by Suppressing Destructive Interference between Charge-Transfer Pathways

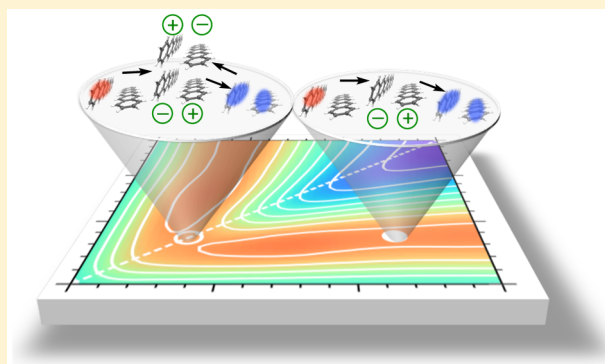
Maria A. Castellanos<sup>†,‡</sup> and Pengfei Huo<sup>\*,†,‡</sup>

<sup>†</sup>Department of Chemistry, University of Rochester, 120 Trustee Road, Rochester, New York 14627, United States

<sup>‡</sup>Department of Chemistry, Universidad Icesi, Cali, Colombia

**S** Supporting Information

**ABSTRACT:** We apply a real-time path-integral approach to investigate the charge-transfer (CT)-mediated singlet fission quantum dynamics in a model pentacene dimer. Our path-integral method gives reliable fission dynamics across various reaction regimes as well as a broad range of reorganization energies and temperatures. With this method, we investigated the destructive interference between the two CT-mediated fission pathways and discovered two mechanisms that can suppress this deleterious effect. First, increasing the energy gap between the two CT states effectively shuts down the high-lying CT pathway, leaving a better functioning low-lying CT pathway with a minimum amount of destructive interference. Second, intermolecular vibrations induce electronic coupling fluctuations, such that the destructive cancellations due to the different signs in static electronic couplings are suppressed. Our numerical results suggest that these two effects can enhance the fission rate up to three times. These findings reveal promising design principles for more efficient singlet fission materials.



Singlet fission (SF) is a photophysical process that converts one singlet excitation into two triplet excitations.<sup>1–4</sup> Combined with acceptor materials that can efficiently convert triplet excitations into separate electron–hole pairs,<sup>5</sup> SF-based photovoltaics can overcome the Shockley–Queisser limit<sup>6</sup> and significantly improve the power conversion efficiency.<sup>7–9</sup> Thus, the SF process provides a promising strategy for designing more efficient solar cells. The fission process has been extensively investigated recently with polyacenes and other organic molecules in the crystalline phase,<sup>10–12</sup> thin film,<sup>13–16</sup> solution,<sup>17,18</sup> and dimeric systems.<sup>19–24</sup>

The essential diabatic electronic states during SF in a dimeric system are summarized in Figure 1. During the initial short-time dynamics of SF, the singlet Frenkel excitonic (FE) states (red) are converted into a correlated triplet–triplet (TT) pair state (blue). In this TT state, two triplet excitations are strongly coupled and the overall spin state is singlet; thus, SF is a spin-allowed process at early stage. The subsequent separation of two triplets is relatively slow<sup>25–27</sup> and is not considered in this work. In the TT state, each triplet excitation has roughly half of the energy compared to the singlet excitation, and the energy of the TT state is close (within  $\pm 300$  meV in polyacenes<sup>28</sup>) to the initial singlet state. In addition, charge-transfer (CT) states (green), that is, CA and AC states, are directly coupled to both singlet and triplet states and play an essential role during the fission process. We shall emphasize that FE and CT states illustrated in Figure 1 are diabatic states and cannot be observed directly in spectroscopy measurements. Experimen-

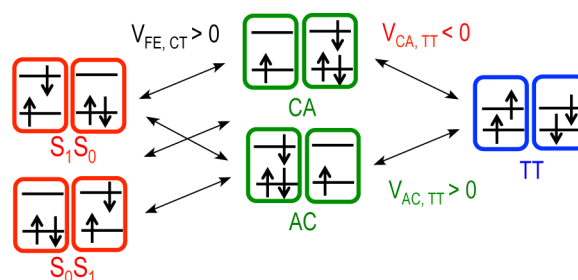


**Figure 1.** Schematic illustration of the relevant diabatic states for SF in a pentacene dimer. During the CT-mediated SF process, singlet FE states ( $S_1S_0$  and  $S_0S_1$ ) are converted into a correlated TT pair state through virtual CT states (CA and AC). The corresponding electronic couplings among these states are labeled by double-sided arrows. Note that the CA–TT and AC–TT couplings have opposite signs.

tally observed states are excitonic states, which are eigenstates of the electronic part of the Hamiltonian and can be expressed as linear combinations of FE and CT states (or so-called singlet states with CT characters<sup>1,4</sup>).

Recent theoretical investigations suggest that the SF process in most polyacenes occurs through the CT-mediated mechanism<sup>1,4,29,30</sup> by using CT states as virtual states to

**Received:** April 20, 2017

**Accepted:** May 18, 2017

**Published:** May 18, 2017

connect FE and TT states. Thus, the CT states can mediate the fission dynamics through two virtual electron-transfer processes between FE and CT states and between CT and TT states. On the other hand, direct conversion of the singlet excitation into the TT pair state, that is, the direct SF mechanism through a simultaneous two-electron process, is less favorable. This is due to the fact that FE–TT electronic couplings (two-electron integrals) are much smaller<sup>1,29</sup> compared to FE–CT and CT–TT electronic couplings (one-electron integrals).

Interestingly, the two CT-mediated fission pathways in pentacene dimer exhibit a large *destructive interference effect*, such that the fission process with two available CT pathways is even slower than that with only one CT pathway.<sup>29,31</sup> This is due to the opposite sign between CA–TT and AC–TT electronic couplings, which originates from the symmetry of the frontier orbitals in polyacene molecules.<sup>1,29,32</sup> Recent theoretical<sup>31</sup> and experimental<sup>13</sup> works also suggest that this destructive interference effect might explain the slower SF rate in the single-crystal phase compared to polycrystalline phases.<sup>31</sup> Similar types of destructive interference effects have been widely observed in electron transfer through bridge states<sup>33,34</sup> and molecular junctions,<sup>35,36</sup> excitation energy transfer between multichromophore light-harvesting complexes,<sup>38</sup> exciton-coupled electron transfer in photosynthetic reaction centers,<sup>37</sup> CT-mediated excitation transfer in organic aggregates,<sup>39,40</sup> and charge recombination processes in photovoltaic heterojunctions.<sup>41</sup> Interference effects have also been discovered between the direct and CT-mediated pathways in SF.<sup>42–45</sup> More efficient fission materials can be obtained through design strategies that minimize these existing destructive interference effects.

Here, we apply a partial-linearized density matrix (PLDM) path-integral method<sup>46</sup> to explore mechanisms that can minimize destructive interference effects in a model pentacene dimer. PLDM is an approximated real-time path-integral approach, which is based on the initial value representation<sup>47</sup> that transforms the path integration into initial condition samplings followed by dynamical propagations. It has been successfully applied to investigate excitation energy transfer<sup>38,46,48</sup> and CT processes<sup>49</sup> and is shown here to reliably describe the nonadiabatic SF dynamics at various reaction regimes as well as over a broad range of solvent reorganization energies and temperatures. With this accurate nonadiabatic dynamics method, we discovered two possible mechanisms that can significantly reduce the destructive interference effect and enhance the fission dynamics.

**Model System.** We use a system–bath model Hamiltonian<sup>50</sup>

$$\hat{H} = \hat{H}_e + \hat{H}_{\text{en}} + \hat{H}_n \quad (1)$$

to explore the SF process in a pentacene dimer. The electronic part of the Hamiltonian  $\hat{H}_e$  includes the energies of the diabatic states and the electronic couplings between them

$$\hat{H}_e = \sum_i |i\rangle E_i \langle i| + \sum_{i \neq j} |i\rangle V_{ij} \langle j| \quad (2)$$

For the pentacene dimer studied here, we consider five diabatic states  $|i\rangle$ , including singlet FE states  $|S_1S_0\rangle$  and  $|S_0S_1\rangle$ , CT states  $|CA\rangle$  and  $|AC\rangle$ , and triplet–triplet pair state  $|TT\rangle$ . The electronic Hamiltonian  $\hat{H}_e$  in this diabatic representation can be further written as

$$\begin{array}{ccccc} |S_1S_0\rangle & |S_0S_1\rangle & |CA\rangle & |AC\rangle & |TT\rangle \\ \begin{bmatrix} E_{S_1S_0} & 0 & t_{LL} & -t_{HH} & 0 \\ 0 & E_{S_0S_1} & -t_{HH} & t_{LL} & 0 \\ t_{LL} & -t_{HH} & E_{CA} & 0 & \sqrt{\frac{3}{2}}t_{LH} \\ -t_{HH} & t_{LL} & 0 & E_{AC} & \sqrt{\frac{3}{2}}t_{HL} \\ 0 & 0 & \sqrt{\frac{3}{2}}t_{LH} & \sqrt{\frac{3}{2}}t_{HL} & E_{TT} \end{bmatrix} & & & & \end{array} \quad (3)$$

Here, the electronic couplings between different states are represented by one-electron integrals based on the HOMO–LUMO active space formalism:<sup>1,50</sup>  $V_{CA,S_1S_0} = \langle CA|\hat{H}_e|S_1S_0\rangle = t_{LL}$ ,  $V_{AC,S_1S_0} = \langle AC|\hat{H}_e|S_1S_0\rangle = -t_{HH}$ ,  $V_{CA,TT} = \langle CA|\hat{H}_e|TT\rangle = \sqrt{3/2}t_{LH}$ , and  $V_{AC,TT} = \langle AC|\hat{H}_e|TT\rangle = \sqrt{3/2}t_{HL}$ . These one-electron integrals, such as  $t_{LL}$  and  $t_{LH}$ , represent the couplings between LUMO or HOMO on individual pentacene molecules.<sup>32,42,50</sup> Direct coupling between singlet and TT state  $\langle S_1S_0|\hat{H}_e|TT\rangle$ , which involves two-electron integrals, is assumed to be zero in this study.

The electronic couplings used in this Letter are adapted from a recent Hartree–Fock calculation,<sup>50</sup> and we refer to this model as the HF model. In addition, an alternative set of parameters for  $\hat{H}_e$  can be obtained from the complete active space self-consistent field (CASSCF) calculation with a subsequent diabaticization procedure.<sup>52</sup> We refer to this set of parameters<sup>52</sup> as the CAS model in this paper. These parameters are provided in the [Supporting Information](#).

Interestingly, both models suggest that  $\text{sgn}(V_{CA,TT}) = -\text{sgn}(V_{AC,TT})$ , with  $\text{sgn}(x)$  as the sign function. Following the previous theoretical analysis based on perturbation theory,<sup>50</sup> we can express the approximated effective fission coupling  $V_{\text{SF}}$  as<sup>29,44</sup>

$$\begin{aligned} V_{\text{SF}} &= \mathcal{V}_{CA} + \mathcal{V}_{AC} \\ &= -\frac{V_{S_1S_0,CA}V_{CA,TT}}{E_{CA} - E_{TT}} - \frac{V_{S_1S_0,CA}V_{CA,TT}}{E_{CA} - E_{S_1S_0}} - \frac{V_{S_1S_0,AC}V_{AC,TT}}{E_{AC} - E_{TT}} \\ &\quad - \frac{V_{S_1S_0,AC}V_{AC,TT}}{E_{AC} - E_{S_1S_0}} \end{aligned} \quad (4)$$

Here  $\mathcal{V}_{CA}$  represents the effective SF coupling associated with the CA pathway (second line in eq 4) and  $\mathcal{V}_{AC}$  represents SF coupling associated with the AC pathway (third line in eq 4). With the HF model, we have  $V_{\text{SF}} \approx -10$  meV.<sup>29</sup> We emphasize that the expression for  $V_{\text{SF}}$  is not used in any of our PLDM simulations. It is merely used for the purpose of interpreting our numerical results.

The electron–nuclei interaction  $\hat{H}_{\text{en}}$  is

$$\hat{H}_{\text{en}} = \sum_k \sum_i c_k^{(ii)} \hat{R}_k^{(ii)} |i\rangle \langle i| + \sum_k \sum_{j \neq i} c_k^{(ij)} \hat{R}_k^{(ij)} |i\rangle \langle j| \quad (5)$$

and the nuclear phonon bath Hamiltonian is

$$\hat{H}_n = \sum_k \sum_{ij} \left[ \frac{\hat{P}_k^{(ij)2}}{2} + \frac{1}{2} \omega_k^{(ii)2} \hat{R}_k^{(ij)2} \right].$$

Here, the intramolecular vibrations, or so-called Holstein couplings (diagonal terms in  $\hat{H}_{\text{en}}$ ), fluctuate the energies of FE, CT, and TT states; the intermolecular vibrations, or so-called Peierls couplings (off-diagonal terms in  $\hat{H}_{\text{en}}$ ), modulate the electronic couplings between these states. In this Letter, only the results reported in [Figure 4](#) are obtained with the Peierls coupling model. We assume that each electronic state  $|i\rangle \langle i|$  has its own independent, uncorrelated bath and so does each  $|i\rangle \langle j|$ .

$j\rangle\langle i|$  pair. In atomistic systems, certain phonon modes might be shared among various electronic states (such as CA and AC states) due to the delocalized nature across multiple monomers.<sup>59,60</sup> The consequences from these correlated baths have been recently explored,<sup>61</sup> suggesting minor impact on the fission rate.

The electron–phonon coupling constants  $c_k^{(ij)}$  and the phonon frequency  $\omega_k^{(ij)}$  are sampled from the Debye spectral density

$$J_{ij}(\omega) = \frac{\pi}{2} \sum_k \frac{c_k^{(ij)2}}{\omega_k^{(ij)}} \delta(\omega - \omega_k^{(ij)}) = \frac{2\lambda_{ij}\Omega_{ij}\omega}{\omega^2 + \Omega_{ij}^2} \quad (6)$$

Here,  $\lambda_{ij} = \pi^{-1} \int d\omega J_{ij}(\omega)/\omega = \sum_k c_k^{(ij)2}/2\omega_k^{(ij)2}$  is the reorganization energy that determines the strength of the electron–phonon interaction;  $\Omega_{ij}$  is the characteristic frequency of the phonon bath. We assume that each independent Holstein (diagonal) bath has the same spectral density  $J_{ii}(\omega) = J_H(\omega)$ , with  $\lambda_H(\omega) = 50$  meV<sup>29</sup> and  $\Omega_{ii} = \Omega_H = 180$  meV, that corresponds to C=C stretching frequency.<sup>29</sup> The value for  $\lambda_H$  used here should be viewed as a conservatively small choice, whereas the experimentally estimated value is around 100–150 meV.<sup>62</sup>

For the Peierls modes, the same independent, identical bath assumption has been applied, with  $\lambda_{ij} = \lambda_p(\omega) = 12$  meV and  $\Omega_{ij} = \Omega_p = 18$  meV.<sup>29,55</sup> These values are consistent with recent theoretical investigations for the Peierls modes in polyacenes<sup>54,56</sup> and other organic crystallines.<sup>57,58</sup> Here, we introduce six independent Peierls phonon bath that are bilinearly coupled to  $|S_1S_0\rangle\langle CA|$ ,  $|S_1S_0\rangle\langle AC|$ ,  $|S_0S_1\rangle\langle CA|$ ,  $|S_0S_1\rangle\langle AC|$ ,  $|CA\rangle\langle TTI|$ ,  $|AC\rangle\langle TTI|$ , and their corresponding conjugate terms.

The Debye form of the spectral density is discretized into  $N = 100$  oscillators. The convergence of the quantum dynamics with the number of bath modes has been carefully checked for all of the temperatures and reorganization energies explored in this Letter. The detailed procedure for bath discretization is described in the Supporting Information.

**Partial Linearized Density Matrix (PLDM) Dynamics.** We apply the PLDM path-integral approach to perform quantum dynamics calculations.<sup>38,46</sup> Here, we briefly outline this method. Expressing the total Hamiltonian as  $\hat{H} = \hat{H}_e + \hat{H}_{en} + \hat{H}_n \equiv \sum_{ij} U_{ij}(\hat{R})|i\rangle\langle j| + \hat{H}_n$ , we use the mapping representation of Meyer–Miller–Stock–Thoss (MMST)<sup>63,64</sup> to transform the discrete electronic states into continuous variables  $|i\rangle\langle j| \rightarrow \hat{a}_i^\dagger \hat{a}_j$ , where  $\hat{a}_i^\dagger = 1/\sqrt{2\hbar}(\hat{q}_i - i\hat{p}_i)$ . Expressing the forward and backward propagators in the time-dependent density operator into path-integral formulation and applying a partial linearization approximation<sup>46</sup> only to the nuclear degrees of freedom (DOF), we arrive at the PLDM expression for computing the reduced density matrix<sup>46,48</sup>

$$\begin{aligned} \rho_{i,j}(t) &= \text{Tr}_R[\hat{\rho}(0)e^{i\hat{H}t/\hbar}|i\rangle\langle j|e^{-i\hat{H}t/\hbar}] \\ &\approx \sum_{nl} \int dR \frac{dP}{2\pi\hbar} dq dp dq' dp' G_0 G_0' [\hat{\rho}(0)_{nl}^W] T_{ni} T_{jl}' \end{aligned} \quad (7)$$

where  $T_{ni} = \frac{1}{2}(q_i(t) + ip_i(t))(q_n(0) - ip_n(0))$  is the electronic transition amplitudes, and  $[\hat{\rho}(0)_{nl}^W]$  is the partial Wigner transformation (with respect to the nuclear DOF) of the  $nl$ th matrix element for the initial density operators  $\hat{\rho}(0)$ , which provides the initial distributions of the nuclear DOF.

The Gaussian function  $G_0 = e^{-(1/2)\sum_n(q_n(0)^2 + p_n(0)^2)}$  in eq 7 provides the initial distributions of the electronic mapping DOF. The terms  $G_0'$  and  $T_{jl}'$  are similarly defined for the backward mapping variables. The details for the initial condition sampling are provided in the Supporting Information.

Classical trajectories are used to evaluate the approximate time-dependent reduced density matrix in eq 7, propagated using the following equations of motion<sup>46,48</sup>

$$\begin{aligned} \dot{q}_i &= \partial h_m(R, \mathbf{p}, \mathbf{q})/\partial p_i & \dot{p}_i &= -\partial h_m(R, \mathbf{p}, \mathbf{q})/\partial q_i \\ F(R) &= -\frac{1}{2}\nabla_R(h_m(R, \mathbf{p}, \mathbf{q}) + h_m(R, \mathbf{p}', \mathbf{q}')) \end{aligned} \quad (8)$$

where  $h_m(R, \mathbf{p}, \mathbf{q}) = \frac{1}{2}\sum_{ij} U_{ij}(R)(p_i p_j + q_i q_j)$  is the classical mapping Hamiltonian<sup>46</sup> and  $F(R)$  is the force that acts on the nuclear DOF. Here, we use  $10^6$  trajectories to generate tightly converged populations for eq 7.

The fission rate constant  $k_{PL}$  is obtained by fitting the PLDM population  $\rho_{TT}(t)$  with the following expression:  $\rho_{TT}(t) = a - b \exp(-k_{PL}t)$ . In addition, we use PLDM to compute the time-dependent population flux to the TT state  $\text{Tr}_R[\hat{\rho}(0) \cdot e^{i\hat{H}t/\hbar} \hat{F} e^{-i\hat{H}t/\hbar}]$ . The flux operator is defined as  $\hat{F} = (i/\hbar)[\hat{H}|TT\rangle\langle TT|]$

$$\begin{aligned} \hat{F} &= (i/\hbar)V_{AC,TT}(|AC\rangle\langle TTI| - |TT\rangle\langle AC|) \\ &+ (i/\hbar)V_{CA,TT}(|CA\rangle\langle TTI| - |TT\rangle\langle CA|) \end{aligned} \quad (9)$$

which is the time derivative of the TT state projection operator. The first line of eq 9 corresponds to flux through the AC pathway, and the second line corresponds to flux through the CA pathway.

Recent experimental study<sup>65</sup> suggests that the formation of vibronic state manifolds with a high density of states facilitates the SF process. Our current calculations, however, only provide the electronic dynamics information. Future model studies that incorporate strong vibronic coupling modes<sup>29</sup> (in addition to the smooth Debye spectral density), as well as theoretical explorations that apply MMST mapping representation for vibronic states to provide time-dependent vibronic population dynamics will generate more detailed mechanistic insights for the SF process.

**Fission Dynamics in the Model Pentacene Dimer.** We start with presenting PLDM quantum dynamics results in a model pentacene dimer at  $T = 300$  K with the HF model.

Figure 2A,B presents the PLDM population dynamics results. We plot the population of diabatic states in three collective groups: FE, which includes  $|S_1S_0\rangle$  and  $|S_0S_1\rangle$  states, CT, which includes  $|CA\rangle$  and  $|AC\rangle$  states, and the TT pair, which includes the  $|TT\rangle$  state. In the model system used here, Redfield theory gives accurate quantum dynamics, which agrees well with the numerical exact result due to the small reorganization energy used here ( $\lambda_H = 50$  meV).<sup>29,50</sup> The PLDM calculations provide nearly quantitative agreement with the results obtained from Redfield theory, both in the “superexchange” regime (A) where CT states are higher than both singlet and triplet states (with  $E_{CT} - E_{FE} = 250$  meV and  $E_{CT} - E_{TT} = 500$  meV) and in the “sequential regime” (B) where the energies of CT states lie in between singlet and triplet states (with  $E_{FE} - E_{CT} = 250$  meV and  $E_{CT} - E_{TT} = 250$ ).<sup>29</sup>

Recent theoretical and experimental investigations suggest that the energies of CT states can be tuned in a broad range by changing the relative distance between monomers,<sup>52</sup> the

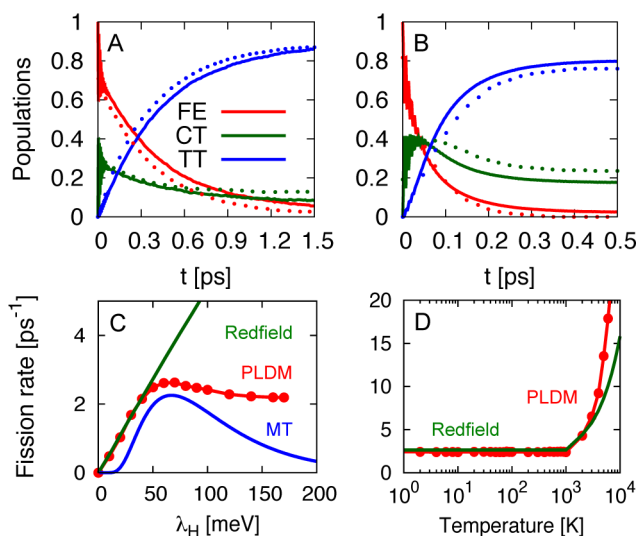


**Figure 2.** Population dynamics and rate constants of SF in a model pentacene dimer. Diabatic populations in (A) superexchange and (B) sequential fission regimes. PLDM results are shown with solid lines, and the results from the Redfield equation<sup>29</sup> are shown with dots. (C) Fission rate as a function of the Holstein solvent reorganization energy  $\lambda_H$ . (D) Fission rate as a function of temperature  $T$ . The rates are obtained with PLDM (red), Redfield theory (green), and Marcus theory (MT) (blue).

relative slip-stacking distance,<sup>70</sup> or the relative orientation between monomers.<sup>71</sup> It is thus important for numerical methods to reliably describe the quantum dynamics in both regimes like what PLDM can provide here.

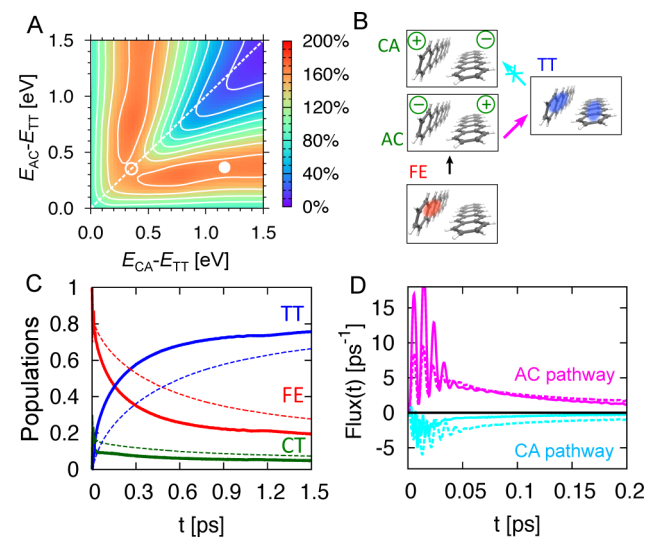
Figure 2C presents the fission rate constant over a range of solvent reorganization energies  $\lambda_H$  of the intramolecular vibrations (Holstein modes). Here, we use the same HF model (in the superexchange regime) as in Figure 2A. In addition, we provide the fission rate estimated from Redfield theory<sup>29</sup> as well as classical Marcus theory (MT).<sup>67–69</sup> The details of these two rate constants and corresponding parameters are provided in the Supporting Information. Redfield theory (green line) gives an accurate rate at small  $\lambda_H$ . However, it starts to break down and fails to predict the correct turnover behavior of the rate at intermediate and large solvent reorganization regimes.<sup>29,44</sup> The fission rate obtained from the PLDM numerical simulations (red dots) gives quantitative agreement with Redfield rate theory at the small  $\lambda_H$  regime and provides correct turnover behavior at intermediate and large  $\lambda_H$  regimes like what MT qualitatively predicts.<sup>44</sup> Note that the intramolecular solvent reorganization energy  $\lambda_H$  in polyacenes is estimated to be  $\sim 100$ – $150$  meV. It is thus important for a quantum dynamics method to provide an accurate rate over a broad range of reorganization energies.

Figure 2D presents the temperature dependency of the fission rate. We use the same parameters for  $\hat{H}_e$  as in Figure 2A. Both PLDM (red) and Redfield theory (green) predict temperature-independent fission dynamics from 0 to 1000 K. Accurate description of the temperature dependency in Figure 2D relies on the preservation of the detailed balance.<sup>66</sup> This is explicitly enforced in Redfield theory (see discussions in the Supporting Information) and approximately achieved in PLDM.<sup>46</sup>

*Destructive Interference Effects between Two CT-Mediated Pathways.* We explore the interference effects between two

CT-mediated fission pathways by varying the energy splitting between CA and AC states over a wide range.

Figure 3A presents the fission yield computed as  $2\rho_{TT}(t)$  after  $t = 0.5$  ps with the HF model.<sup>29</sup> The time-dependent



**Figure 3.** Interference effects between the two CT-mediated SF pathways. (A) SF yield  $2\rho_{TT}(t)$  as a function of  $E_{CA}$  and  $E_{AC}$  after  $t = 0.5$  ps with the HF model. Filled circle:  $E_{CA} - E_{AC} \approx 0.8$  eV. Open circle: with degenerate CT states. (B) Schematic illustration of the destructive interference effect between CA and AC pathways. (C) Population dynamics in the pentacene dimer with the CAS model (solid) and with the m-CAS model (dash). (D) Probability flux to the TT state through AC (magenta) and CA (cyan) pathways, with the CAS (solid) and the m-CAS (dash) models.

fission yield after four periods of time is provided in the Supporting Information. The diagonal dashed line corresponds to the systems with degenerate CT states. Along this line, the fission yield decreases drastically as  $E_{CA}$  and  $E_{AC}$  increase, consistent with previous investigations<sup>29</sup> that suggest that only low-lying CT states can effectively mediate fission as virtual states. The off-diagonal regions correspond to the systems with nondegenerate CT states. The open circle on the diagonal dashed line corresponds to a system with degenerate CT states, and the filled circle corresponds to the system with  $E_{CA} - E_{AC} \approx 0.8$  eV, as indicated by the recent CASSCF calculations<sup>52</sup> for an isolated pentacene dimer.

Interestingly, the system with nondegenerate CT states (off-diagonal regions) has an even higher time-dependent yield compared to the system that has two degenerate low-lying CT states (diagonal dashed line). Comparing the systems indicated with the filled and open circles in Figure 3A, the PLDM fission rate suggests that when only one low-lying CT state is available to mediate fission, the dynamics is two times faster compared to that when two low-lying CT states are available and mediate the fission process. This result clearly demonstrates the destructive interference between the two CT-mediated pathways.<sup>29,31</sup> Previous theoretical studies on the transition dipole moment<sup>53</sup> in pentacene suggest a similar result, in agreement with our finding here.

This interference effect can be understood from the effective fission coupling  $V_{SF} = V_{CA} + V_{AC}$  in eq 4. The fission rate (at the MT level) is proportional to  $|V_{SF}|^2 = V_{CA}^2 + V_{AC}^2 + 2V_{CA}V_{AC}$ . If the fission rate through

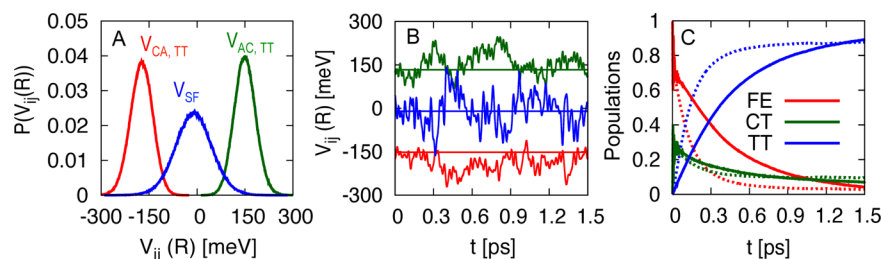


**Figure 4.** Impact of intermolecular vibrations on SF dynamics. (A) Distribution of the Peierls-fluctuated electronic couplings  $V_{ij}(R)$  and effective SF coupling  $V_{SF}(R)$ . (B) Time-dependent  $V_{ij}(R(t))$  and  $V_{SF}(R(t))$  of one representative trajectory. Static values for these electronic couplings are indicated with straight lines. (C) Population dynamics for SF with the Peierls modes (dash) and without the Peierls modes (solid).

the single CT channel is associated with  $\mathcal{V}_{CA}^2$  and  $\mathcal{V}_{AC}^2$  terms, then the cross product term  $2\mathcal{V}_{CA}\mathcal{V}_{AC}$  will give the interference effect.

A careful examination of  $V_{SF}$  in eq 4 reveals a large amount of cancellations between  $\mathcal{V}_{CA}$  and  $\mathcal{V}_{AC}$  due to the opposite sign of CA–TT and AC–TT couplings. The interference contribution  $2\mathcal{V}_{CA}\mathcal{V}_{AC}$  in the rate constant is negative, which reveals the origin of the destructive interference effects observed in Figure 3. Increasing  $E_{CA} - E_{TT}$  and  $E_{CA} - E_{S,S_0}$  in the denominator of the  $\mathcal{V}_{CA}$  term in eq 4 will decrease the contribution associated with the CA state and reduce the amount of destructive cancellations, giving a larger  $V_{SF}$  and faster fission dynamics. Thus, raising the CA state energy to a higher value effectively eliminates this pathway and leaves a better functioning single AC pathway without a large amount of destructive interference.

Figure 3B presents the schematic summary of the observed destructive interference effect. Due to the opposite signs of  $V_{AC,TT}$  and  $V_{CA,TT}$ , keeping both pathways open slows down the fission dynamics. By increasing the energy level of the CA state and essentially eliminating this fission pathway, the dimeric system has a better functioning AC pathway without destructive interference.

To further investigate this destructive interference effect, we consider two sets of model parameters for pentacene. First, we use the CAS model<sup>52</sup> to parametrize  $\hat{H}_e$  in eq 2. This model suggests that in the isolated pentacene dimer the energy of the CA state is about 1.16 eV higher than that of the TT state, whereas the energy of AC is low-lying and only 0.36 eV higher than the TT state.<sup>52</sup> Second, we parametrize  $\hat{H}_e$  with the same CAS parameters except that both CT states are now low-lying and they are degenerate, with  $E_{CA} = E_{AC}$ , and refer to this model as the m-CAS model (modified CAS).

Figure 3C presents the population dynamics with both the CAS model (solid lines) where  $E_{CA} > E_{AC}$  and the m-CAS model (dash lines) where  $E_{CA} = E_{AC}$ . We find that the CT population in the m-CAS model (dash green) is roughly two times larger than the CT population in the CAS model (solid green). This indicates that in the m-CAS model both CA and AC states are populated and able to mediate the fission process, whereas in the CAS model only the low-lying AC state is populated. On the other hand, the CAS model gives much faster fission dynamics compared to the m-CAS model, with about two times enhancement of the fission rate, clearly demonstrating destructive interference effects.<sup>29,31</sup>

Figure 3D presents the PLDM value of the population flux. The flux through the AC pathway (magenta) is positive (forward flux), and the flux through the CA pathway (cyan) is negative (backward flux). The destructive interference effect is clearly demonstrated by the relative magnitude of the

population flux through these two CT channels. In the m-CAS model (dash lines), the forward and backward flux have a similar magnitude, leading to a small forward net flux to the TT state. In the CAS model (solid lines) where there is a large energy gap between CA and AC states, forward flux through the AC pathway becomes much larger and the backward flux through the CA pathway becomes smaller, leading to a larger net forward flux. This flux analysis is also illustrated in Figure 3B.

We need to emphasize that the large splitting between the energies of CA and AC states is a well-known result due to the charge-quadruple interactions in isolated systems,<sup>73–75</sup> which has also been confirmed by other correlated wave function calculations.<sup>72</sup> However, in the single-crystal phase, the dimer will be surrounded by other pentacene molecules, and the electrostatic interactions will decrease the gap between CA and AC states.<sup>73</sup> Thus, one should expect large destructive interference effects for fission dynamics in the pentacene crystal, and we should be cautious in extending our discovery to the fission dynamics in pentacene crystals.

In crystalline pentacene, nearly degenerate CA and AC states caused by electrostatic relaxation<sup>73,76</sup> will lead to large destructive interference.<sup>31</sup> However, this deleterious effect can be alleviated by removing part of the surrounding pentacene molecules,<sup>31</sup> which will partially re-establish the energy gap between CA and AC states and hence reduce the destructive interference. This situation is expected to be typical at crystallite boundaries,<sup>31</sup> in polycrystalline phases and thin films,<sup>13</sup> or at the interface between pentacene and fullerene derivatives in heterojunctions.<sup>8</sup> Recent experimental results in tetracene crystals suggest faster (two to three times enhancement of) fission dynamics in the polycrystalline phase than that in the single-crystalline phase.<sup>13</sup> One possible explanation<sup>31</sup> is that in the polycrystalline phase the energy gap between CT states is enlarged due to the locally broken crystal symmetry, reducing destructive interference effects and enhancing the fission process. Further interpretation of experimental results requires additional theoretical work.

*Impact of Intermolecular Vibrations on SF.* We investigate the impact of intermolecular vibrations on fission dynamics, which remained to be carefully examined.<sup>29,57,77</sup> Intermolecular vibrations can modulate the relative stacking configurations of pentacene monomers, leading to fluctuating electronic couplings between FE, CT, and TT states. Recent theoretical investigations discovered that in SF crystals<sup>54,56</sup> and phthalocyanine molecular crystals<sup>58</sup> electronic couplings can exhibit large fluctuations due to the intermolecular vibrations.

Here, we use the HF model to parametrize  $\hat{H}_e$ , the same as in Figure 2A. We assume that two CT states have degenerate energy levels in order to explore the individual impact from

intermolecular vibrations on fission dynamics. We use the off-diagonal Peierls phonon bath described in eq 5 to model these intermolecular vibrations and explore their impact on fission dynamics. The Peierls-fluctuated electronic couplings  $V_{ij}(R)$  (for  $i \neq j$ ) can be expressed as

$$V_{ij}(R) = \langle i|\hat{H}_e + \hat{H}_{\text{en}}|j\rangle = V_{ij} + \sum_k c_k^{(ij)} R_k^{(ij)} \quad (10)$$

where  $V_{ij} = \langle i|\hat{H}_e|j\rangle$  is the static value of electronic couplings defined in eq 2. The variance  $\sigma_{ij}^2$  characterizes the distribution of  $V_{ij}(R)$  around its static value  $V_{ij}$  as follows

$$\sigma_{ij}^2 = \langle V_{ij}^2(R) \rangle_{\text{P}} - V_{ij}^2 \quad (11)$$

where  $\langle \dots \rangle_{\text{P}}$  represents the ensemble average with respect to the Peierls-fluctuated electronic Hamiltonian  $V_{ij}(R)$ . Note that with the system–bath model used here, we have  $\langle V_{ij}(R) \rangle_{\text{P}} = V_{ij}$ , and these variances can be evaluated analytically with the detailed expressions provided in the Supporting Information.

Figure 4A presents the distribution of the Peierls-fluctuated electronic coupling  $V_{ij}(R)$  computed from eq 10. Here, we focus on two particular couplings:  $V_{\text{CA,TT}}(R)$  (red) and  $V_{\text{AC,TT}}(R)$  (green); each one has a distribution with  $\sigma_{ij}^2 = 31.7$  meV. Further, we compute the Peierls-fluctuated effective fission coupling  $V_{\text{SF}}(R)$  (blue) based on the expression in eq 4 by replacing  $V_{ij}$  with  $V_{ij}(R)$ . As  $V_{\text{SF}}(R)$  contains products of two electronic couplings and each one of them has a Gaussian distribution,  $V_{\text{SF}}(R)$  has a distribution of the Meijer  $G$  function<sup>78</sup> with  $\sigma_{\text{eff}} = 51.3$  meV, broader than the Gaussian distribution for individual  $V_{ij}(R)$ .

Figure 4B presents the time-dependent values of  $V_{ij}(R)$  and  $V_{\text{SF}}(R)$  of one representative trajectory. The static electronic couplings are also presented with straight solid lines. Peierls phonons can fluctuate the instantaneous value of electronic couplings around their static values. These fluctuations in  $V_{ij}(R)$ , depending on their instantaneous signs and values, can reduce the destructive interference and alleviate the net cancellations among individual terms in  $V_{\text{SF}}(R)$  (see eq 4), leaving a fluctuated  $V_{\text{SF}}(R)$  with a broad distribution. The large instantaneous value of  $V_{\text{SF}}(R)$  can be viewed as “dynamical hot spots”, which can promote fission processes. Thus, one should expect more efficient fission dynamics with the presence of the Peierls modes.

Figure 4C presents a comparison of the population dynamics for the system with (dashed lines) and without (solid lines) the Peierls modes. The presence of the Peierls modes enhances the fission rate by almost three times (based on the rate estimated from the TT population) and causes a rapid rise of the TT population within the first 200 fs. These results support our hypothesis that fluctuations in  $V_{ij}(R)$  reduce the destructive interference between the two CT pathways. Note that Peierls couplings physically exist in the real system; modeling SF without including these modes in pentacene will underestimate the fission rate. Without Peierls couplings, the theoretical fission time ( $1/k_{\text{SF}}$ ) based on the HF model is around 500 fs, approximately two to three times slower compared to experimental values.<sup>29</sup> When we do explicitly incorporate Peierls couplings, however, our theoretical fission time based on the HF model system agrees well with experimental values that range from 80 to 200 fs.<sup>7,10</sup>

Previously developed rate theory<sup>79,80</sup> that explicitly considers the Peierls fluctuations can provide further insight for the enhanced fission dynamics. This theory suggests that the rate is

dictated by the square average coupling  $\langle V_{\text{SF}}^2(R) \rangle_{\text{P}} = V_{\text{SF}}^2 + \sigma_{\text{SF}}^2$ , not just the static electronic coupling  $V_{\text{SF}}$ . In the model study here, the Peierls modes induce large structural fluctuations that contribute to the  $\sigma_{\text{SF}}^2$  term, leading to an enhanced fission process. A similar rate enhancement mechanism due to large structure fluctuations has also been extensively explored in the context of electron-transfer dynamics in proteins.<sup>81,82</sup> However, the importance of such effects in the context of SF has just begun to emerge.<sup>57</sup>

The previous theoretical study based on Redfield theory suggests a minimal role of the Peierls couplings in SF dynamics,<sup>29</sup> which contradicts our results here. We believe that this contradiction is due to the fundamental limitation of Redfield theory. In the pentacene dimer, the low-frequency Peierls modes are off-resonance with the energy gaps between excitonic states, leading to nearly zero contribution in the Redfield rate constant. However, by incorporating these off-diagonal Peierls modes as *static disorders* in  $\hat{H}_e$  instead, the Peierls averaged Redfield rate predicts a similar amount of enhancement for fission, in agreement with our path-integral results. These analyses based on modified Redfield theory are provided in the Supporting Information.

Finally, we performed detailed studies on the temperature dependency of the fission dynamics in pentacene dimer with Peierls phonons. Our PLDM simulation results suggest that even with these Peierls modes the fission process in the pentacene dimer exhibits a very weak temperature dependency. On the other hand, when static electronic couplings  $V_{ij}$  are exactly zero due to the packing symmetry, for example, in  $C_{2h}$   $\pi$ -stacked pentacene or rubrene,<sup>77</sup> the only contribution to  $V_{\text{SF}}(R)$  comes from Peierls fluctuations and our numerical results show a strong temperature dependency and a thermally activated fission process. These results and additional theoretical analysis based on modified Redfield theory are provided in the Supporting Information.

While the dimeric system is often used as an approximated description for a realistic crystal system, it cannot describe the delocalization of the singlet and TT states, nor it can properly describe the mixture of singlet and CT states due to the surrounding monomers.<sup>51</sup> Future quantum dynamics simulations will focus on incorporating these effects in a realistic crystal model.<sup>51</sup>

In this Letter, we apply an accurate nonadiabatic path-integral method to investigate the SF dynamics in the pentacene dimer. Our results clearly demonstrate the destructive interference effects between CT-mediated fission pathways. We discovered two potential mechanisms that can significantly suppress this deleterious effect. First, increasing the energetic splitting of the CT states will reduce the destructive interference between them, leaving a better functioning pathway that can mediate fission dynamics more efficiently. We expect this mechanism to be feasible in isolated dimer systems as well as at crystallite boundaries.<sup>31</sup> Second, intermolecular vibrations induce fluctuations in electronic couplings. These fluctuations will significantly reduce cancellations of static electronic coupling terms between the two CT pathways in the effective fission coupling expression and result in a more efficient fission process controlled by a broad distribution of the fission coupling. This effect has been overlooked due to the limitation of Redfield theory.<sup>29</sup> Together, these results shed light on how to take advantage of intrinsic features in fission materials, such as the energy splitting between CT states or intermolecular vibrations, to reduce the

existing destructive interference and enhance SF dynamics. These discoveries might also provide useful design principles for more efficient fission devices and SF-based photovoltaics.

## ■ ASSOCIATED CONTENT

### Supporting Information

The Supporting Information is available free of charge on the ACS Publications website at DOI: 10.1021/acs.jpcllett.7b00972.

Parameters for the electronic Hamiltonian, additional results on reducing destructive interference effects, the time-dependent SF yield, Peierls-modified Marcus–Hush and Redfield theory, and temperature dependent studies of the model system with the Peierls phonons and two different packing configurations (PDF)

## ■ AUTHOR INFORMATION

### Corresponding Author

\*E-mail: pengfei.huo@rochester.edu.

### ORCID

Pengfei Huo: 0000-0002-8639-9299

### Notes

The authors declare no competing financial interest.

## ■ ACKNOWLEDGMENTS

This work was supported by the University of Rochester startup funds. Computing resources were provided by the Center for Integrated Research Computing (CIRC) at the University of Rochester. The authors thank Dr. Farnaz Shakib and Rachel Clune for helpful comments and a thorough reading of this manuscript. M.A.C. appreciates the Summer Research Fellowships for International Students from the University of Rochester. P.H. appreciates valuable discussions with Profs. Frank Spano, David Beratan, and Xiao-Yang Zhu.

## ■ REFERENCES

- (1) Smith, M.; Michl, J. Recent Advances in Singlet Fission. *Annu. Rev. Phys. Chem.* **2013**, *64*, 361–386.
- (2) Smith, M.; Michl, J. Singlet Fission. *Chem. Rev.* **2010**, *110*, 6891–6936.
- (3) Zimmerman, P. M.; Zhang, Z.; Musgrave, C. B. Singlet Fission in Pentacene through Multi-exciton Quantum States. *Nat. Chem.* **2010**, *2*, 648–652. Zimmerman, P. M.; Bell, F.; Casanova, D.; Head-Gordon, M. Mechanism for Singlet Fission in Tetracene and Pentacene: from Single Exciton to Two Triplets. *J. Am. Chem. Soc.* **2011**, *133*, 19944–19952.
- (4) Monahan, N.; Zhu, X.-Y. Charge Transfer-Mediated Singlet Fission. *Annu. Rev. Phys. Chem.* **2015**, *66*, 601–618.
- (5) Congreve, D. N.; Lee, J.; Thompson, N. J.; Hontz, E.; Yost, S. R.; Reuswig, P. D.; Bahlke, M. E.; Reineke, S.; Van Voorhis, T.; Baldo, M. A. External Quantum Efficiency above 100% in a Singlet-Exciton Fission-Based Organic Photovoltaic Cell. *Science* **2013**, *340*, 334–337.
- (6) Shockley, W.; Queisser, H. J. Detailed Balance Limit of Efficiency of p-n Junction Solar Cells. *J. Appl. Phys.* **1961**, *32*, 510–519.
- (7) Chan, W.-L.; Ligges, M.; Jailaubekov, A.; Kaake, L.; Miaja-Avila, L.; Zhu, X.-Y. Observing the Multiexciton State in Singlet Fission and Ensuing Ultrafast Multielectron Transfer. *Science* **2011**, *334*, 1541–1545.
- (8) Lee, J.; Jadhav, P.; Reuswig, P. D.; Yost, S. R.; Thompson, N. J.; Congreve, D. N.; Hontz, E.; Van Voorhis, T.; Baldo, M. A. Singlet Exciton Fission Photovoltaics. *Acc. Chem. Res.* **2013**, *46*, 1300–1311.
- (9) Akimov, A. V.; Prezhdov, O. V. Nonadiabatic Dynamics of Charge Transfer and Singlet Fission at the Pentacene/C60 Interface. *J. Am. Chem. Soc.* **2014**, *136*, 1599–1608.
- (10) Wilson, M. W. B.; Rao, A.; Clark, J.; Kumar, R. S.; Brida, D.; Cerullo, G.; Friend, R. H. Ultrafast Dynamics of Exciton Fission in Polycrystalline Pentacene. *J. Am. Chem. Soc.* **2011**, *133*, 11830–11833.
- (11) Chan, W.-L.; Ligges, M.; Zhu, X.-Y. The Energy Barrier in Singlet Fission can be Overcome through Coherent Coupling and Entropic Gain. *Nat. Chem.* **2012**, *4*, 840–845.
- (12) Wan, Y.; Guo, Z.; Zhu, T.; Yan, S.; Johnson, J.; Huang, L. Cooperative Singlet and Triplet Exciton Transport in Tetracene Crystals Visualized by Ultrafast Microscopy. *Nat. Chem.* **2015**, *7*, 785–792. Roberts, S. T. Energy transport: Singlet to triplet and back again. *Nat. Chem.* **2015**, *7*, 764–765.
- (13) Piland, G. B.; Bardeen, C. J. How Morphology Affects Singlet Fission in Crystalline Tetracene. *J. Phys. Chem. Lett.* **2015**, *6*, 1841–1846.
- (14) Le, A. K.; Bender, J. A.; Roberts, S. T. Slow Singlet Fission Observed in a Perylenediimide Thin Film. *J. Phys. Chem. Lett.* **2016**, *7*, 4922–4928.
- (15) Eaton, S. E.; Shoer, L. E.; Karlen, S. D.; Dyar, S. M.; Margulies, E. A.; Veldkamp, B. S.; Ramanan, C.; Hartzler, D. A.; Savikhin, S.; Marks, T. J.; et al. Singlet Exciton Fission in Polycrystalline Thin Films of a Slip-Stacked Perylenediimide. *J. Am. Chem. Soc.* **2013**, *135*, 14701–14712.
- (16) Burdett, J. J.; Müller, A. M.; Gosztoła, D.; Bardeen, C. J. Excited state dynamics in solid and monomeric tetracene: The roles of superradiance and exciton fission. *J. Chem. Phys.* **2010**, *133*, 144506/1–144506/12.
- (17) Walker, B. J.; Musser, A. J.; Beljonne, D.; Friend, R. H. Singlet exciton fission in solution. *Nat. Chem.* **2013**, *5*, 1019–1024.
- (18) Zhang, Y.-D.; Wu, Y.; Xu, Y.; Wang, Q.; Liu, K.; Chen, J.-W.; Cao, J.-J.; Zhang, C.; Fu, H.; Zhang, H.-L. Excessive Exoergicity Reduces Singlet Exciton Fission Efficiency of Heteroacenes in Solutions. *J. Am. Chem. Soc.* **2016**, *138*, 6739–6745.
- (19) Müller, A. M.; Avlasevich, Y. S.; Schoeller, W. W.; Müllen, K.; Bardeen, C. J. Exciton Fission and Fusion in Bis(tetracene) Molecules with Different Covalent Linker Structures. *J. Am. Chem. Soc.* **2007**, *129*, 14240–14250.
- (20) Korovina, N. V.; Das, S.; Nett, Z.; Feng, X.; Joy, J.; Haiges, R.; Krylov, A. I.; Bradforth, S. E.; Thompson, M. E. Singlet Fission in a Covalently Linked Cofacial Alkynyltetracene Dimer. *J. Am. Chem. Soc.* **2016**, *138*, 617–627.
- (21) Zirzmeier, J.; Lehnerr, D.; Coto, P. B.; Chernick, E. T.; Casillas, R.; Basel, B. S.; Thoss, M.; Tykwinski, R. R.; Guldi, D. M. Singlet fission in pentacene dimers. *Proc. Natl. Acad. Sci. U. S. A.* **2015**, *112*, 5325–5330.
- (22) Sanders, S. N.; Kumarasamy, E.; Pun, A. B.; Appavoo, K.; Steigerwald, M. L.; Campos, L. M.; Sfeir, M. Y. Exciton Correlations in Intramolecular Singlet Fission. *J. Am. Chem. Soc.* **2016**, *138*, 7289–7297.
- (23) Fuemmeler, S. E. G.; Sanders, N.; Pun, A. B.; Kumarasamy, E.; Zeng, T.; Miyata, K.; Steigerwald, M. L.; Zhu, M. Y.; Sfeir, M. Y.; Campos, L. M.; Ananth, N. A Direct Mechanism of Ultrafast Intramolecular Singlet Fission in Pentacene Dimers. *ACS Cent. Sci.* **2016**, *2*, 316–324.
- (24) Varnavski, O.; Abeyasinghe, N.; Arago, J.; Serrano-Perez, J. J.; Orti, E.; Lopez Navarrete, J. T.; Takimiya, K.; Casanova, D.; Casado, J.; Goodson, T. High Yield Ultrafast Intramolecular Singlet Exciton Fission in a Quinoidal Bithiophene. *J. Phys. Chem. Lett.* **2015**, *6*, 1375–1384.
- (25) Pensack, R. D.; Ostroumov, E. E.; Tilley, A. J.; Mazza, S.; Grieco, C.; Thorley, K. J.; Asbury, J. B.; Seferos, D. S.; Anthony, J. E.; Scholes, G. D. Observation of Two Triplet-Pair Intermediates in Singlet Exciton Fission. *J. Phys. Chem. Lett.* **2016**, *7*, 2370–2375.
- (26) Scholes, G. D. Correlated Pair States Formed by Singlet Fission and Exciton-Exciton Annihilation. *J. Phys. Chem. A* **2015**, *119*, 12699–12705.
- (27) Piland, G. B.; Burdett, J. J.; Dillon, R. J.; Bardeen, C. J. Singlet Fission: From Coherences to Kinetics. *J. Phys. Chem. Lett.* **2014**, *5*, 2312–2319.

- (28) Busby, E.; Berkelbach, T. C.; Kumar, B.; Chernikov, A.; Zhong, Y.; Hlaing, H.; Zhu, X.-Y.; Heinz, T. F.; Hybertsen, M. S.; Sfeir, M. Y.; Reichman, D. R.; et al. Multiphonon Relaxation Slows Singlet Fission in Crystalline Hexacene. *J. Am. Chem. Soc.* **2014**, *136*, 10654–10660.
- (29) Berkelbach, T. C.; Hybertsen, M. S.; Reichman, D. R. Microscopic theory of singlet exciton fission. II. Application to pentacene dimers and the role of superexchange. *J. Chem. Phys.* **2013**, *138*, 114103/1–114103/12.
- (30) Greyson, E. C.; Vura-Weis, J.; Michl, J.; Ratner, M. A. Maximizing Singlet Fission in Organic Dimers: Theoretical Investigation of Triplet Yield in the Regime of Localized Excitation and Fast Coherent Electron Transfer. *J. Phys. Chem. B* **2010**, *114*, 14168–14177.
- (31) Petelenz, P.; Snamina, M. Locally Broken Crystal Symmetry Facilitates Singlet Exciton Fission. *J. Phys. Chem. Lett.* **2016**, *7*, 1913–1916.
- (32) Wang, L.; Olivier, Y.; Prezhdo, O. V.; Beljonne, D. Maximizing Singlet Fission by Intermolecular Packing. *J. Phys. Chem. Lett.* **2014**, *5*, 3345–3353.
- (33) Goldsmith, R. H.; Wasielewski, M. R.; Ratner, M. A. Electron Transfer in Multiply Bridged Donor-Acceptor Molecules: Dephasing and Quantum Coherence. *J. Phys. Chem. B* **2006**, *110*, 20258–20262.
- (34) Zarea, M.; Powell, D.; Renaud, N.; Wasielewski, M. R.; Ratner, M. A. Decoherence and Quantum Interference in a Four-Site Model System: Mechanisms and Turnovers. *J. Phys. Chem. B* **2013**, *117*, 1010–1020.
- (35) Chen, S.; Zhang, Y.; Koo, S.; Tian, H.; Yam, C.; Chen, G.; Ratner, M. A. Interference and Molecular Transport—A Dynamical View: Time-Dependent Analysis of Disubstituted Benzenes. *J. Phys. Chem. Lett.* **2014**, *5*, 2748–2752.
- (36) Frisenda, R.; Janssen, V. A. E. C.; Grozema, F. C.; van der Zant, H. S. J.; Renaud, N. Mechanically controlled quantum interference in individual  $\pi$ -stacked dimers. *Nat. Chem.* **2016**, *8*, 1099–1104.
- (37) Renaud, N.; Powell, D.; Zarea, M.; Movaghar, B.; Wasielewski, M. R.; Ratner, M. A. Quantum Interferences and Electron Transfer in Photosystem I. *J. Phys. Chem. A* **2013**, *117*, 5899–5908.
- (38) Huo, P.; Miller, T. F., III. Electronic coherence and the kinetics of inter-complex energy transfer in light-harvesting systems. *Phys. Chem. Chem. Phys.* **2015**, *17*, 30914–30924.
- (39) Yamagata, H.; Pochas, C. M.; Spano, F. C. Designing J- and H-Aggregates through Wave Function Overlap Engineering: Applications to Poly (3-hexylthiophene). *J. Phys. Chem. B* **2012**, *116*, 14494–14503.
- (40) Hestand, N. J.; Spano, F. C. Interference between Coulombic and CT-mediated couplings in molecular aggregates: H-to J-aggregate transformation in perylene-based  $\pi$ -stacks. *J. Chem. Phys.* **2015**, *143*, 244707/1–244707/16.
- (41) Tempelaar, R.; Koster, L. J. A.; Havenith, R. W. A.; Knoester, J.; Jansen, T. L. C. Charge Recombination Suppressed by Destructive Quantum Interference in Heterojunction Materials. *J. Phys. Chem. Lett.* **2016**, *7*, 198–203.
- (42) Renaud, N.; Grozema, F. C. Intermolecular Vibrational Modes Speed Up Singlet Fission in Perylenediimide Crystals. *J. Phys. Chem. Lett.* **2015**, *6*, 360–365.
- (43) Renaud, N.; Sherratt, P. A.; Ratner, M. A. Mapping the Relation between Stacking Geometries and Singlet Fission Yield in a Class of Organic Crystals. *J. Phys. Chem. Lett.* **2013**, *4*, 1065–1069.
- (44) Tao, G. Understanding Electronically Non-Adiabatic Relaxation Dynamics in Singlet Fission. *J. Chem. Theory Comput.* **2015**, *11*, 28–36.
- (45) Tao, G. Electronically Nonadiabatic Dynamics in Singlet Fission: A Quasi-Classical Trajectory Simulation. *J. Phys. Chem. C* **2014**, *118*, 17299–17305.
- (46) Huo, P.; Coker, D. F. Communication: Partial linearized density matrix dynamics for dissipative, non-adiabatic quantum evolution. *J. Chem. Phys.* **2011**, *135*, 201101/1–201101/4.
- (47) Miller, W. H. The Semiclassical Initial Value Representation: A Potentially Practical Way for Adding Quantum Effects to Classical Molecular Dynamics Simulations. *J. Phys. Chem. A* **2001**, *105*, 2942–2955.
- (48) Lee, M.; Huo, P.; Coker, D. F. Semi-classical path integral dynamics: Photosynthetic energy transfer with realistic environment interactions. *Annu. Rev. Phys. Chem.* **2016**, *67*, 639–668.
- (49) Huo, P.; Miller, T. F.; Coker, D. F. Communication: Predictive partial linearized path integral simulation of condensed phase electron transfer dynamics. *J. Chem. Phys.* **2013**, *139*, 151103/1–151103/4.
- (50) Berkelbach, T. C.; Hybertsen, M. S.; Reichman, D. R. Microscopic theory of singlet exciton fission. I. General formulation. *J. Chem. Phys.* **2013**, *138*, 114102/1–114102/16.
- (51) Berkelbach, T. C.; Hybertsen, M. S.; Reichman, D. R. Microscopic theory of singlet exciton fission. III. Crystalline pentacene. *J. Chem. Phys.* **2014**, *141*, 074705/1–074705/12.
- (52) Zeng, T.; Hoffmann, R.; Ananth, N. The Low-Lying Electronic States of Pentacene and Their Roles in Singlet Fission. *J. Am. Chem. Soc.* **2014**, *136*, 5755–5764.
- (53) Beljonne, D.; Yamagata, H.; Brédas, J. L.; Spano, F. C.; Olivier, Y. Charge-Transfer Excitations Steer the Davydov Splitting and Mediate Singlet Exciton Fission in Pentacene. *Phys. Rev. Lett.* **2013**, *110*, 226402/1–226402/5.
- (54) Ito, S.; Nagami, T.; Nakano, M. Density Analysis of Intra- and Intermolecular Vibronic Couplings toward Bath Engineering for Singlet Fission. *J. Phys. Chem. Lett.* **2015**, *6*, 4972–4977.
- (55) Girlando, A.; Grisanti, L.; Masino, M.; Brillante, A.; Della Valle, R. G.; Venuti, E. Interaction of charge carriers with lattice and molecular phonons in crystalline pentacene. *J. Chem. Phys.* **2011**, *135*, 084701/1–084701/6.
- (56) Aragón, J.; Troisi, A. Dynamics of the Excitonic Coupling in Organic Crystals. *Phys. Rev. Lett.* **2015**, *114*, 026402/1–026402/5.
- (57) Renaud, N.; Grozema, F. C. Intermolecular Vibrational Modes Speed Up Singlet Fission in Perylenediimide Crystals. *J. Phys. Chem. Lett.* **2015**, *6*, 360–365.
- (58) Fornari, R. P.; Aragón, J.; Troisi, A. Exciton Dynamics in Phthalocyanine Molecular Crystals. *J. Phys. Chem. C* **2016**, *120*, 7987–7996.
- (59) Yao, Y. Coherent dynamics of singlet fission controlled by nonlocal electron-phonon coupling. *Phys. Rev. B: Condens. Matter Mater. Phys.* **2016**, *93*, 115426/1–115426/6.
- (60) Li, Y.; Coropceanu, V.; Brédas, J.-L. Nonlocal electron-phonon coupling in organic semiconductor crystals: The role of acoustic lattice vibrations. *J. Chem. Phys.* **2013**, *138*, 204713/1–204713/6.
- (61) Fujihashi, Y.; Ishizaki, A. Fluctuations in Electronic Energy Affecting Singlet Fission Dynamics and Mixing with Charge-Transfer State: Quantum Dynamics Study. *J. Phys. Chem. Lett.* **2016**, *7*, 363–369.
- (62) Kera, S.; Hosoumi, S.; Sato, K.; Fukagawa, H.; Nagamatsu, S.; Sakamoto, Y.; Suzuki, T.; Huang, H.; Chen, W.; Thye Shen Wee, A.; et al. Experimental Reorganization Energies of Pentacene and Perfluoropentacene: Effects of Perfluorination. *J. Phys. Chem. C* **2013**, *117*, 22428–22437.
- (63) Meyer, H. D.; Miller, W. H. A classical analog for electronic degrees of freedom in nonadiabatic collision processes. *J. Chem. Phys.* **1979**, *70*, 3214–3223.
- (64) Stock, G.; Thoss, M. Semiclassical description of nonadiabatic quantum dynamics. *Phys. Rev. Lett.* **1997**, *78*, 578–581; Mapping approach to the semiclassical description of nonadiabatic quantum dynamics. *Phys. Rev. A: At, Mol, Opt. Phys.* **1999**, *59*, 64–79.
- (65) Bakulin, A. A.; Morgan, S. E.; Kehoe, T. B.; Wilson, M. W. B.; Chin, A. W.; Zigmantas, D.; Egorova, D.; Rao, A. Real-time observation of multiexcitonic states in ultrafast singlet fission using coherent 2D electronic spectroscopy. *Nat. Chem.* **2015**, *8*, 16–23.
- (66) Chan, W.-C.; Berkelbach, T. C.; Provorse, M. R.; Monahan, N. R.; Tritsch, J. R.; Hybertsen, M. S.; Reichman, D. R.; Gao, J.; Zhu, X.-Y. The Quantum Coherent Mechanism for Singlet Fission: Experiment and Theory. *Acc. Chem. Res.* **2013**, *46*, 1321–1329.
- (67) Yost, S. R.; Lee, J.; Wilson, M. W. B.; Wu, T.; McMahon, D. P.; Parkhurst, R. R.; Thompson, N. J.; Congreve, D. N.; Rao, A.; Johnson, K.; et al. A transferable model for singlet-fission kinetics. *Nat. Chem.* **2014**, *6*, 492–497.

- (68) Teichen, P. E.; Eaves, J. D. A Microscopic Model of Singlet Fission. *J. Phys. Chem. B* **2012**, *116*, 11473–11481.
- (69) Teichen, P. E.; Eaves, J. D. Collective aspects of singlet fission in molecular crystals. *J. Chem. Phys.* **2015**, *143*, 044118/1–044118/16.
- (70) Margulies, E. A.; Miller, C. E.; Wu, Y.; Ma, L.; Schatz, G. C.; Young, R. M.; Wasielewski, M. R. Enabling singlet fission by controlling intramolecular charge transfer in  $\pi$ -stacked covalent terrylenediimide dimers. *Nat. Chem.* **2016**, *8*, 1120–1125.
- (71) Cook, R. E.; Phelan, B. T.; Kamire, R. J.; Majewski, B. M.; Young, R. M.; Wasielewski, M. R. Excimer Formation and Symmetry-Breaking Charge Transfer in Cofacial Perylene Dimers. *J. Phys. Chem. A* **2017**, *121*, 1607–1615.
- (72) Coto, P. B.; Sharifzadeh, S.; Neaton, J. B.; Thoss, M. Low-Lying Electronic Excited States of Pentacene Oligomers: A Comparative Electronic Structure Study in the Context of Singlet Fission. *J. Chem. Theory Comput.* **2015**, *11*, 147–156.
- (73) Petelenz, P.; Snamina, M.; Mazur, G. Charge-Transfer States in Pentacene: Dimer versus Crystal. *J. Phys. Chem. C* **2015**, *119*, 14338–14342.
- (74) Petelenz, P.; Snamina, M. Charge-Transfer Coupling of an Embedded Pentacene Dimer with the Surrounding Crystal Matrix. *J. Phys. Chem. C* **2015**, *119*, 28570–28576.
- (75) Beljonne, D.; Cornil, J.; Muccioli, L.; Zannoni, C.; Bredas, J.-L.; Castet, F. Electronic Processes at Organic–Organic Interfaces: Insight from Modeling and Implications for Opto-electronic Devices. *Chem. Mater.* **2011**, *23*, 591–609.
- (76) Parker, S. M.; Seideman, T.; Ratner, M. A.; Shiozaki, T. Model Hamiltonian Analysis of Singlet Fission from First Principles. *J. Phys. Chem. C* **2014**, *118*, 12700–12705.
- (77) Tamura, H.; Huix-Rotllant, M.; Burghardt, I.; Olivier, Y.; Beljonne, D. First-Principles Quantum Dynamics of Singlet Fission: Coherent versus Thermally Activated Mechanisms Governed by Molecular  $\pi$  Stacking. *Phys. Rev. Lett.* **2015**, *115*, 107401/1–107401/5.
- (78) Springer, M. D.; Thompson, W. E. The Distribution of Products of Beta, Gamma and Gaussian Random Variables. *SIAM J. Appl. Math.* **1970**, *18*, 721–737.
- (79) Troisi, A.; Nitzan, A.; Ratner, M. A. A rate constant expression for charge transfer through fluctuating bridges. *J. Chem. Phys.* **2003**, *119*, 5782–5788.
- (80) Goychuk, I. A.; Petrov, E. G.; May, V. Bridge-assisted electron transfer driven by dichotomically fluctuating tunneling coupling. *J. Chem. Phys.* **1995**, *103*, 4937–4944.
- (81) Beratan, D. N.; Skourtis, S. S.; Balabin, I. A.; Balaeff, A.; Keinan, S.; Venkatramani, R.; Xiao, D. Steering Electrons on Moving Pathways. *Acc. Chem. Res.* **2009**, *42*, 1669–1678.
- (82) Medvedev, D. M.; Daizadeh, I.; Stuchebrukhov, A. A. Electron Transfer Tunneling Pathways in Bovine Heart Cytochrome c Oxidase. *J. Am. Chem. Soc.* **2000**, *122*, 6571–6582.